



HAL
open science

Minimum-Energy Path Generation for a Quadrotor UAV

Fabio Morbidi, Roel Cano, David Lara

► **To cite this version:**

Fabio Morbidi, Roel Cano, David Lara. Minimum-Energy Path Generation for a Quadrotor UAV. IEEE International Conference on Robotics and Automation, May 2016, Stockholm, Sweden. hal-01276199v2

HAL Id: hal-01276199

<https://hal.science/hal-01276199v2>

Submitted on 27 Dec 2016

HAL is a multi-disciplinary open access archive for the deposit and dissemination of scientific research documents, whether they are published or not. The documents may come from teaching and research institutions in France or abroad, or from public or private research centers.

L'archive ouverte pluridisciplinaire **HAL**, est destinée au dépôt et à la diffusion de documents scientifiques de niveau recherche, publiés ou non, émanant des établissements d'enseignement et de recherche français ou étrangers, des laboratoires publics ou privés.

Minimum-Energy Path Generation for a Quadrotor UAV

Fabio Morbidi, Roel Cano, David Lara

Abstract—A major limitation of existing battery-powered quadrotor UAVs is their reduced flight endurance. To address this issue, by leveraging the electrical model of a brushless DC motor, we explicitly determine minimum-energy paths between a predefined initial and final configuration of a quadrotor by solving an optimal control problem with respect to the angular accelerations of the four propellers. As a variation on this problem, if the total energy consumption between two boundary states is *fixed*, minimum-time and/or minimum-control-effort trajectories are computed for the aerial vehicle. The theory is illustrated for the DJI Phantom 2 quadrotor in three realistic scenarios.

I. INTRODUCTION

A. Motivation and related work

In spite of the recent large-scale diffusion of rotary-wing micro Unmanned Aerial Vehicles (UAVs), whose number of rotors ranges between four and eight depending on the payload and demanded redundancy, these systems still suffer from a major limitation: the *reduced flight endurance*, typically between 15 and 30 minutes. Some promising new applications (package delivery, cinematography, aerial manipulation) have lately emerged: however, the limited runtime of the existing lithium-ion polymer (LiPo) batteries strongly restricts the class of missions that a rotorcraft can successfully carry out.

To alleviate this problem for *quadrotors*, the simplest and most popular class of rotary-wing micro UAVs, a significant effort has been invested in weight reduction by adopting carbon-fiber airframes and high-energy-density soft-pouch battery packages, and in the improvement of power-to-weight ratio of brushless DC motors, which are the main responsible for energy consumption. These efforts have been successful in reducing operation in power-starved regimes: nevertheless, no technological breakthrough is expected along these lines in the near future. Building upon commercial off-the-shelf aerial platforms, it has then become imperative to devise novel *algorithm-level* solutions to save energy and extend endurance. In this paper, we will focus on the *path-planning problem* and by introducing suitable optimal control problems with respect to the angular accelerations of the four motors, we will compute minimum-energy and fixed-energy trajectories for a quadrotor.

Several solutions contributing towards increased endurance have been recently proposed in the literature. These solutions have mainly focused on the improvement of the mechanical design and of the power system of a quadrotor. For instance, more efficient rotor configurations have been explored in [1] (triangular arrangement with propellers of different diameter) and in [2] (tilting motors guaranteeing

actuation redundancy). However, both designs are still at a prototype stage. In [3], the authors have described an energy-efficient aerial platform developed using a minimalistic design approach, whereas in [4], a simple model is introduced to estimate the endurance of a quadrotor exploring an indoor environment, and a ceiling attachment is proposed as a means of preserving energy while maintaining a bird's eye view. Abdilla *et al.* have provided a characterization of the energy consumption of a rotorcraft powered by LiPo batteries in stable hovering flight, and introduced a more accurate endurance estimation model tailored to the Parrot AR.Drone 2.0 [5]. Other recent studies have envisaged to extend UAVs' mission time by dumping exhausted battery modules out of the aircraft in flight, thus reducing the mass of the vehicle [6]. Nevertheless, environmental and safety concerns will likely prevent the large-scale adoption of this solution in civilian applications. Aerial robots tethered to a ground station have lately become a viable option. The tether can be used to provide energy to the aircraft, thus offering virtually unlimited flight time (see, e.g. [7] and the references therein). Finally, in [8], [9] automatic battery change/recharge platforms have been developed to enable long-endurance missions for multiple quadrotors.

The problem of generating *energy-optimal paths* for a rotorcraft has received much less attention in the aerial-robotics literature. In [10] an energy-efficient path-planning strategy has been proposed for a hexarotor on a multi-target mission. However, differently from our work, the authors relied on an approximated energy cost function which does not explicitly depend on the physical parameters of the electrical motors. Moreover, unlike [10], where a heuristic procedure is utilized to numerically solve a generalized version of the Travelling Salesman Problem on a reduced four-dimensional space, we provide a 6-DOF path generator.

B. Original contributions and organization

Taking inspiration from [11], where energy-optimal trajectories are determined for a double-integrator wheeled robot, in this paper we obtain minimum-energy paths between two given boundary states for a quadrotor UAV by solving a new optimal control problem with respect to the angular accelerations of the four brushless DC motors. If the energy one expects to consume in flight is *fixed* a priori, minimum-time and/or minimum-control-effort trajectories are also computed by solving a related optimal control problem with a scalar isoperimetric constraint. A simple strategy for estimating the state of charge of the battery once the quadrotor has reached the end state, is also discussed. In order to simplify the analysis, in this work we will assume that the four motors are the only responsible for the energy consumed by the quadrotor: in other words, the impact of the ESC (Electronic Speed Controller), microcontroller, and on-board sensors on energy balance will be neglected. To illustrate the theory, the energy-optimal trajectories of the DJI Phantom 2 quadrotor are

F. Morbidi is with the MIS laboratory, Université de Picardie Jules Verne, 33, rue Saint-Leu, 80039 Amiens, France. Email: fabio.morbidi@u-picardie.fr

R. Cano and D. Lara are with the Universidad Autónoma de Tamaulipas, Posgrado-UAMRR, GPO Box 1460, Reynosa Tamps. Mexico, CP 88779.

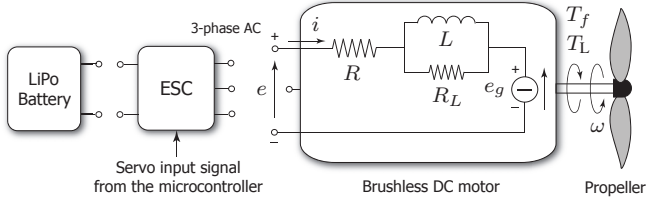


Fig. 1. Electrical model of the brushless DC motor of a quadrotor UAV.

numerically computed with the ACADO Toolkit [12] in a variety of real-world scenarios.

The rest of this paper is organized as follows. Sect. II presents the electrical model of a brushless DC motor and the dynamic model of a quadrotor UAV. In Sect. III, the minimum-energy and fixed-energy path generation problems are formulated, and in Sect. IV, the results of extensive numerical experiments conducted with the Phantom 2 are discussed. Finally, in Sect. V the main contributions of the paper are summarized and some possible avenues for future research are outlined.

II. PRELIMINARIES

A. Electrical model of a brushless DC motor

The model for a battery-powered brushless DC motor takes into account the energy dissipated in the resistive and inductive windings, and the energy required to overcome the internal and load friction. The instantaneous current $i(t)$ in the motor (see Fig. 1), is given by [13], [14],

$$i(t) = \frac{1}{K_T} [T_f + T_L(\omega(t)) + D_f \omega(t) + (J_m + J_L) \frac{d\omega(t)}{dt}], \quad (1)$$

where $\omega(t)$ is the angular velocity of the motor shaft [rad/s], K_T is the torque constant of the motor [Nm/A], T_f is the motor friction torque, $T_L(\omega(t))$ is the speed-dependent load friction torque which results from propeller drag, D_f is the viscous damping coefficient of the motor [Nms/rad], and J_m , J_L are the motor and load moments of inertia, respectively. Note that in a brushless DC motor, T_f is small (usually only due to bearing drag), and D_f , which is due to energy losses in liquid lubrication, is very small as well. The voltage across the motor $e(t)$ is given by (cf. Fig. 1):

$$e(t) = Ri(t) + K_E \omega(t) + L \frac{di(t)}{dt}, \quad (2)$$

where R and L are the resistance and inductance of phase winding, respectively, and K_E is the voltage constant of the motor [Vs/rad]. Note that $K_E = K_T$ [13, p. 2-7]: in addition, if K_E is expressed in mV/rpm, we have that $K_E = 1000/K_V$ where K_V is the motor velocity constant [rpm/V]. With reference to Fig. 1, note that the resistance R_L , representing the losses in the magnetic circuit of the motor, is usually much larger than R (typically about 5-10 times): hence, the effect of R_L on motor operation can be neglected [13]. Under steady-state conditions, the current $i(t)$ is constant, and equation (2) reduces to:

$$e(t) = Ri(t) + K_E \omega(t). \quad (3)$$

where $e_g(t) = K_E \omega(t)$ is the counter electromotive force of the motor.

Remark 1: For the sake of simplicity, in our electrical model we neglected the effect of the ESC between the LiPo battery and the brushless motor (see Fig. 1), and the energy lost through inefficiencies in the battery. We also assumed that the shaft of the motor is directly connected to the propeller (i.e. no gearbox). This is typically the case in commercial quadrotors (DJI Phantom 2 and 3, AscTec Pelican, and Parrot Bebop). \diamond

B. Quadrotor dynamic model

Let $\mathbf{q} = [x, y, z]^T$ be the position vector of the center of mass of the quadrotor relative to the fixed inertial frame $\{\mathcal{E}\}$. The quadrotor's Euler angles (the orientation of the vehicle) are expressed by $\Phi = [\phi, \theta, \psi]^T$ where ϕ is the roll angle about the x -axis, θ the pitch angle about the y -axis, and ψ the yaw angle about the z -axis (see Fig. 2). Four identical brushless DC motors are attached to the rigid cross airframe of the quadrotor: motor 1 and 3 rotate counterclockwise (with reference to the positive direction of the z -axis of the body-fixed frame $\{\mathcal{B}\}$), while motor 2 and 4 rotate clockwise with an angular velocity $\omega_j \geq 0$, generating a thrust f_j , $j \in \{1, 2, 3, 4\}$ in free air (see Fig. 2). The full dynamic model of the quadrotor is given by [15], [16]:

$$\begin{cases} m \ddot{x} = (\sin \phi \sin \psi + \cos \phi \cos \psi \sin \theta) u_1, \\ m \ddot{y} = (\cos \phi \sin \theta \sin \psi - \cos \psi \sin \phi) u_1, \\ m \ddot{z} = (\cos \theta \cos \phi) u_1 - mg, \\ I_x \ddot{\phi} = (I_y - I_z) \dot{\theta} \dot{\psi} + \ell u_2 - J \dot{\theta} u_5, \\ I_y \ddot{\theta} = (I_z - I_x) \dot{\phi} \dot{\psi} + \ell u_3 + J \dot{\phi} u_5, \\ I_z \ddot{\psi} = (I_x - I_y) \dot{\phi} \dot{\theta} + u_4, \end{cases} \quad (4)$$

where $u_1 \triangleq \kappa_b (\omega_1^2 + \omega_2^2 + \omega_3^2 + \omega_4^2)$, $u_2 \triangleq \kappa_b (\omega_2^2 - \omega_4^2)$, $u_3 \triangleq \kappa_b (\omega_3^2 - \omega_1^2)$, $u_4 \triangleq \kappa_\tau (\omega_1^2 + \omega_3^2 - \omega_2^2 - \omega_4^2)$, $u_5 \triangleq \omega_1 - \omega_2 + \omega_3 - \omega_4$. In (4), m denotes the mass of the quadrotor in kilograms, $g = 9.8066 \text{ m/s}^2$ is the acceleration due to gravity, $\mathbb{I} = \text{diag}(I_x, I_y, I_z)$ is the diagonal rotational inertia matrix of the rotorcraft expressed in $\{\mathcal{B}\}$, $J \triangleq J_m + J_L$ is the total inertia of a motor, ℓ is the distance between each motor and the center of mass of the quadrotor (i.e. half of the wheelbase), and κ_b, κ_τ in u_1, \dots, u_4 are the thrust and aerodynamic drag factors of the propellers, respectively.

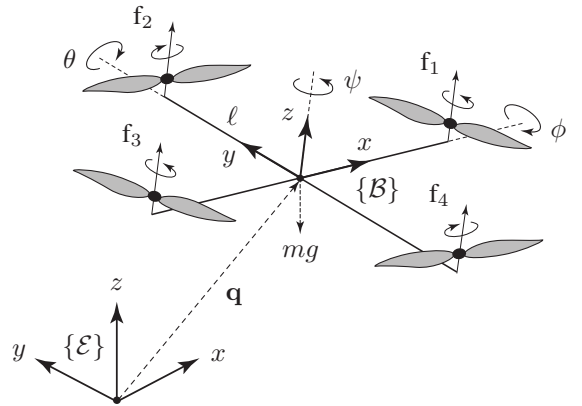


Fig. 2. Inertial frame $\{\mathcal{E}\}$ and body-fixed frame $\{\mathcal{B}\}$ of the quadrotor, and Euler angles ϕ , θ and ψ .

Following [17] and [18, Sect. 2.5], we have that:

$$\begin{aligned} J_L &= \frac{1}{4} n_B m_B (r - \epsilon)^2, \\ \kappa_b &= C_T \rho A r^2, \quad \kappa_\tau = C_Q \rho A r^3, \end{aligned} \quad (5)$$

where n_B is the number of blades of the propeller, m_B is the blade mass, r and $A = \pi r^2$ are the radius and disk area of the propeller, respectively, ϵ is the offset between the blade root and the motor hub, C_T is the nondimensional thrust coefficient of the propeller (which depends on propeller geometry and profile), $C_Q = C_T \sqrt{C_T}/2$ is the torque coefficient of the propeller, and ρ is the density of air.

III. DETERMINATION OF MINIMUM-ENERGY PATHS

In this section we introduce the optimal control problem that is instrumental in determining the minimum-energy control input of the quadrotor UAV. Let $e_j(t)$ and $i_j(t)$ denote the voltage (in volts) and current (in amperes) across motor $j \in \{1, 2, 3, 4\}$ of the quadrotor at time t . The energy consumed by the vehicle between the initial time t_0 and the fixed end time t_f is then,

$$E = \int_{t_0}^{t_f} \sum_{j=1}^4 e_j(t) i_j(t) dt. \quad (6)$$

By using equations (1) and (3) for the four identical motors, and by noticing that $T_L(\omega_j(t)) = \kappa_\tau \omega_j^2(t)$, $j \in \{1, 2, 3, 4\}$ [17], we can rewrite equation (6) as follows:

$$E = \int_{t_0}^{t_f} \sum_{j=1}^4 [c_1 + c_2 \omega_j(t) + c_3 \omega_j^2(t) + c_4 \omega_j^3(t) + c_5 \omega_j^4(t) + c_6 \dot{\omega}_j(t) + c_7 \dot{\omega}_j^2(t) + c_8 \omega_j(t) \dot{\omega}_j(t) + c_9 \omega_j^2(t) \dot{\omega}_j(t)] dt, \quad (7)$$

where $\dot{\omega}_j(t)$ is the angular acceleration of motor j , and c_1, c_2, \dots, c_9 are constants depending on the parameters of the motors and on the geometry of the propeller, given by,

$$\begin{aligned} c_1 &= \frac{R T_f^2}{K_T^2}, \quad c_2 = \frac{T_f}{K_T} \left(\frac{2 R D_f}{K_T} + K_E \right), \\ c_3 &= \frac{D_f}{K_T} \left(\frac{R D_f}{K_T} + K_E \right) + \frac{2 R T_f \kappa_\tau}{K_T^2}, \\ c_4 &= \frac{\kappa_\tau}{K_T} \left(\frac{2 R D_f}{K_T} + K_E \right), \quad c_5 = \frac{R \kappa_\tau^2}{K_T^2}, \quad c_6 = \frac{2 R J T_f}{K_T^2}, \\ c_7 &= \frac{R J^2}{K_T^2}, \quad c_8 = \frac{J}{K_T} \left(\frac{2 R D_f}{K_T} + K_E \right), \quad c_9 = \frac{2 R J \kappa_\tau}{K_T^2}. \end{aligned}$$

Remark 2 (Simplified energy model): Note that,

$$\begin{aligned} &\int_{t_0}^{t_f} \sum_{j=1}^4 [c_6 \dot{\omega}_j(t) + c_8 \omega_j(t) \dot{\omega}_j(t) + c_9 \omega_j^2(t) \dot{\omega}_j(t)] dt \\ &= \sum_{j=1}^4 [c_6 (\omega_j(t_f) - \omega_j(t_0)) + \frac{c_8}{2} (\omega_j^2(t_f) - \omega_j^2(t_0)) \\ &\quad + \frac{c_9}{3} (\omega_j^3(t_f) - \omega_j^3(t_0))]. \end{aligned}$$

If we now assume that $\omega_j(t_0) = \omega_j(t_f)$, $\forall j \in \{1, 2, 3, 4\}$, i.e., the initial and final angular velocities of each motor are identical (thus constraining the class of maneuvers our path generator will exploit), then (7) simply reduces to:

$$E_r = \int_{t_0}^{t_f} \sum_{j=1}^4 [c_1 + c_2 \omega_j(t) + c_3 \omega_j^2(t) + c_4 \omega_j^3(t) + c_5 \omega_j^4(t) + c_7 \dot{\omega}_j^2(t)] dt. \quad (8)$$

This simplified expression for the energy will be used in the rest of this paper \diamond

Our ultimate goal is to cast the minimum-energy path generation problem for a quadrotor UAV as a standard optimal control problem [19]. To this end, we rewrite system (4) in state-space form by introducing the *state vector* $\mathbf{x} = [x_1, x_2, \dots, x_{16}]^T \in \mathbb{R}^{16}$ and the *input vector* $\boldsymbol{\alpha} = [\alpha_1, \alpha_2, \alpha_3, \alpha_4]^T \in \mathbb{R}^4$, defined as follows:

$$\begin{aligned} x_1 &= x, \quad x_2 = \dot{x}_1 = \dot{x}, \quad x_3 = y, \quad x_4 = \dot{x}_3 = \dot{y}, \\ x_5 &= z, \quad x_6 = \dot{x}_5 = \dot{z}, \quad x_7 = \phi, \quad x_8 = \dot{x}_7 = \dot{\phi}, \\ x_9 &= \theta, \quad x_{10} = \dot{x}_9 = \dot{\theta}, \quad x_{11} = \psi, \quad x_{12} = \dot{x}_{11} = \dot{\psi}, \\ x_{13} &= \omega_1, \quad \dot{x}_{13} = \alpha_1, \quad x_{14} = \omega_2, \quad \dot{x}_{14} = \alpha_2, \\ x_{15} &= \omega_3, \quad \dot{x}_{15} = \alpha_3, \quad x_{16} = \omega_4, \quad \dot{x}_{16} = \alpha_4. \end{aligned}$$

With this change of variables, the following system of first-order differential equations is obtained:

$$\begin{cases} \dot{x}_1 = x_2, \\ \dot{x}_2 = \frac{\kappa_b}{m} (\sin x_7 \sin x_{11} + \cos x_7 \cos x_{11} \sin x_9) \sum_{k=13}^{16} x_k^2, \\ \dot{x}_3 = x_4, \\ \dot{x}_4 = \frac{\kappa_b}{m} (\cos x_7 \sin x_9 \sin x_{11} - \cos x_{11} \sin x_7) \sum_{k=13}^{16} x_k^2, \\ \dot{x}_5 = x_6, \\ \dot{x}_6 = \frac{\kappa_b}{m} (\cos x_9 \cos x_7) \sum_{k=13}^{16} x_k^2 - g, \\ \dot{x}_7 = x_8, \\ \dot{x}_8 = \left(\frac{I_y - I_z}{I_x} \right) x_{10} x_{12} + \frac{\ell \kappa_b}{I_x} (x_{14}^2 - x_{16}^2) \\ \quad - \frac{J}{I_x} x_{10} (x_{13} - x_{14} + x_{15} - x_{16}), \\ \dot{x}_9 = x_{10}, \\ \dot{x}_{10} = \left(\frac{I_z - I_x}{I_y} \right) x_8 x_{12} + \frac{\ell \kappa_b}{I_y} (x_{15}^2 - x_{13}^2) \\ \quad + \frac{J}{I_y} x_8 (x_{13} - x_{14} + x_{15} - x_{16}), \\ \dot{x}_{11} = x_{12}, \\ \dot{x}_{12} = \left(\frac{I_x - I_y}{I_z} \right) x_8 x_{10} + \frac{\kappa_\tau}{I_z} (x_{13}^2 - x_{14}^2 + x_{15}^2 - x_{16}^2), \\ \dot{x}_{13} = \alpha_1, \quad \dot{x}_{14} = \alpha_2, \quad \dot{x}_{15} = \alpha_3, \quad \dot{x}_{16} = \alpha_4. \end{cases} \quad (9)$$

Note that thanks to the ‘‘auxiliary’’ state variables x_{13}, \dots, x_{16} , the nonlinear system (9) is *affine in the control* $\boldsymbol{\alpha}$, i.e. it is of the form $\dot{\mathbf{x}} = \mathbf{F}(\mathbf{x}) + \mathbf{G} \boldsymbol{\alpha}$ where the vector field $\mathbf{F}(\mathbf{x}) : \mathbb{R}^{16} \rightarrow \mathbb{R}^{16}$ and $\mathbf{G} = [\mathbf{0}_{4 \times 12} \quad \mathbf{I}_{4 \times 4}]^T$, being $\mathbf{0}_{4 \times 12}$ the 4×12 matrix of zeros and $\mathbf{I}_{4 \times 4}$ the 4×4 identity matrix. With the cost function (8) and system (9) at hand, we are now in a position to introduce the following optimal control problem:

$$\begin{aligned} \min_{\substack{\alpha_1, \alpha_2 \\ \alpha_3, \alpha_4}} E_r &= \int_{t_0}^{t_f} \left[\sum_{k=13}^{16} (c_1 + c_2 x_k(t) + c_3 x_k^2(t) \right. \\ &\quad \left. + c_4 x_k^3(t) + c_5 x_k^4(t)) + c_7 \sum_{j=1}^4 \alpha_j^2(t) \right] dt \\ \text{s.t.} \quad &\text{System (9), } \mathbf{x}(t_0) = \mathbf{x}_{t_0}, \quad \mathbf{x}(t_f) = \mathbf{x}_{t_f}, \end{aligned}$$

$$\begin{aligned}
0 &\leq x_{13} \leq \omega_{\max}, & 0 &\leq x_{14} \leq \omega_{\max}, \\
0 &\leq x_{15} \leq \omega_{\max}, & 0 &\leq x_{16} \leq \omega_{\max},
\end{aligned} \tag{10}$$

where $\omega_{\max} > 0$ is the maximum motor speed, and $\mathbf{x}_{t_0}, \mathbf{x}_{t_f} \in \mathbb{R}^{16}$ are assigned boundary state vectors. Note that the last four components of $\mathbf{x}_{t_0}, \mathbf{x}_{t_f}$ must match in order to satisfy the assumption of Remark 2. The numerical solution to problem (10) will be discussed in Sect. IV.

Remark 3 (Battery state-of-charge estimation): For $t \in [t_0, t_f]$, let $i_{\text{dis}}(t) = [\sum_{k=13}^{16} (T_f + \kappa_\tau x_k^2(t) + D_f x_k(t)) + J \sum_{j=1}^4 \alpha_j(t)] / K_T$ be the discharge current of the battery of the quadrotor *along the minimum-energy path*, determined by solving problem (10). Given $i_{\text{dis}}(t)$ for $t \in [t_0, t_f]$, the state of charge of the battery can be estimated via the following simple “two-well” kinetic battery model (or KiBaM in short) [20, Sect. 3]:

$$\begin{aligned}
\dot{y}_1(t) &= -i_{\text{dis}}(t) + k_F(h_2(t) - h_1(t)), \\
\dot{y}_2(t) &= -k_F(h_2(t) - h_1(t)),
\end{aligned} \tag{11}$$

with initial conditions $y_1(t_0) = \gamma C$, $y_2(t_0) = (1 - \gamma) C$, where C is the total capacity of the battery in ampere-second, and $\gamma > 0$ gives the fraction of the total capacity of the battery that is put in the so-called available-charge well. Moreover, y_1, y_2 indicate the amount of charge stored in the available- and bound-charge wells, respectively, k_F [Hz] is a parameter controlling the rate at which the charge flows between the two wells, and $h_1 = y_1/\gamma$, $h_2 = y_2/(1 - \gamma)$. The battery is considered empty (fully discharged) when there is no charge left in the available-charge well, i.e. $y_1 = 0$. \diamond

A. Trajectories at fixed energy

In this section, we study a variation on problem (10). Let us suppose that the total energy supply between two boundary states of the quadrotor is *fixed* and equal to E_{tot} . Then, the space of *isoenergetic paths* between time t_0 and t_f , is given by $\mathcal{S} = \{\mathbf{x}(t) : [t_0, t_f] \rightarrow \mathbb{R}^{16}, \boldsymbol{\alpha}(t) : [t_0, t_f] \rightarrow \mathbb{R}^4 \mid (\mathbf{x}, \boldsymbol{\alpha}) \text{ satisfy (9), } \mathbf{x}(t_0) = \mathbf{x}_{t_0}, \mathbf{x}(t_f) = \mathbf{x}_{t_f}, E_r = E_{\text{tot}}\}$. In order to single out a specific path in \mathcal{S} , taking inspiration from (10), we introduce the following optimal control problem:

$$\begin{aligned}
&\min_{\alpha_1, \alpha_2, \alpha_3, \alpha_4, t_f} \int_{t_0}^{t_f} [\eta + \boldsymbol{\alpha}^T(t) \mathbf{Q} \boldsymbol{\alpha}(t)] dt \\
&\text{s.t.} \quad \text{System (9), } \mathbf{x}(t_0) = \mathbf{x}_{t_0}, \mathbf{x}(t_f) = \mathbf{x}_{t_f}, \\
&\quad \dot{x}_{17} = \sum_{k=13}^{16} (c_1 + c_2 x_k + c_3 x_k^2 \\
&\quad \quad \quad + c_4 x_k^3 + c_5 x_k^4) + c_7 \sum_{j=1}^4 \alpha_j^2, \\
&\quad x_{17}(t_0) = 0, \quad x_{17}(t_f) = E_{\text{tot}}, \\
&\quad 0 \leq x_{13} \leq \omega_{\max}, \quad 0 \leq x_{14} \leq \omega_{\max}, \\
&\quad 0 \leq x_{15} \leq \omega_{\max}, \quad 0 \leq x_{16} \leq \omega_{\max}.
\end{aligned} \tag{12}$$

Note that for the sake of generality, in (12) we chose a cost function that is a weighted combination of elapsed time and control effort, being $\mathbf{Q} \in \mathbb{R}^{4 \times 4}$ a symmetric positive semidefinite gain matrix. We also remark that differently from problem (10), whereas t_0 is fixed, the end time t_f is now *free*. In the cost function, $\eta > 0$ is used to weigh the relative importance of elapsed time and control effort:

in fact, for $\eta \rightarrow 0$ we obtain an open-end-time minimum-control-effort problem, while for $\eta \rightarrow \infty$ the optimal solution resembles a minimum-time solution [19, Sect. 5.5]. As in problem (10), the last four components of $\mathbf{x}_{t_0}, \mathbf{x}_{t_f}$ must match in order to satisfy the condition of Remark 2. Note that following [21, Sect. 3.5], in problem (12) the *isoperimetric constraint* $E_r = E_{\text{tot}}$ has been treated as a terminal-state equality constraint by defining the new state component x_{17} whose differential equation is $\dot{x}_{17} = \sum_{k=13}^{16} (c_1 + c_2 x_k + c_3 x_k^2 + c_4 x_k^3 + c_5 x_k^4) + c_7 \sum_{j=1}^4 \alpha_j^2$, and set $x_{17}(t_f) - E_{\text{tot}} = 0$.

IV. NUMERICAL EXPERIMENTS

Problem (10) and (12) have been numerically solved using the ACADO Toolkit [12] for Matlab. For the optimization routines, the default options in ACADO were considered: thus, a multiple-shooting discretization with 20 nodes was utilized and the integration was performed with a Runge-Kutta method (order 4/5). The optimization of the discretized mathematical program was based on a sequential quadratic programming (SQP) method. Finally, the KKT tolerance used for the convergence criterion of the SQP algorithm was set to 10^{-5} in all our tests, and the maximum number of iterations was fixed to 40.

As a case study, in our tests we considered the DJI Phantom 2 quadrotor [22] with E300 Multirotor Propulsion System (2212/920KV motors), powered by a 3-cell (3S) LiPo 11.1 V battery with capacity $C = 18720$ As. The physical parameters of the Phantom 2 used in the three scenarios discussed below, are reported in Table I. The majority of these parameters, which are instrumental in computing c_1, c_2, \dots, c_5 , and c_7 in (8), were found in Phantom 2’s User Manual: for the missing ones, we relied on the values reported in [23], [24] for similar quadrotors. Note that the inertia J_m of the outrunner motors was computed using the inertia formula of a thin cylindrical shell with open ends of radius r_{rot} and mass m_{rot} , i.e. $J_m = m_{\text{rot}} r_{\text{rot}}^2$. We assumed that the weight of the rotating part of the motor is 50% of the total weight. Finally, the constants J_L, κ_b and κ_τ were computed using the formulae in (5).

A. Scenario 1: variable end states

In the first scenario, we numerically solved problem (10) with a number of control (or integration) intervals equal to 100, to find the minimum-energy input that drives the quadrotor from the origin at time $t_0 = 0$ s, to the eight vertices of a parallelepiped of side 8, 10 and 6 m, at time $t_f = 20$ s. More precisely, we set,

$K_V = 920$ rpm/V	$n_B = 2$	$\rho = 1.225$ kg/m ³
$K_E = 9.5493/K_V$ Vs/rad	$m_B = 0.0055$ kg	$m = 1.3$ kg
$T_f = 4 \times 10^{-2}$ Nm	$r = 0.12$ m	$\ell = 0.175$ m
$D_f = 2 \times 10^{-4}$ Nms/rad	$\epsilon = 0.004$ m	$I_x = 0.081$ kgm ²
$R = 0.2$ Ω	$C_T = 0.0048$	$I_y = 0.081$ kgm ²
$J_m = 4.9 \times 10^{-6}$ kgm ²	$C_Q = 2.3515 \times 10^{-4}$	$I_z = 0.142$ kgm ²
$\omega_{\max} = 1047.197$ rad/s	$r_{\text{rot}} = 0.014$ m	$m_{\text{rot}} = 0.025$ kg

TABLE I
PARAMETERS OF THE PHANTOM 2 USED IN THE
NUMERICAL EXPERIMENTS.

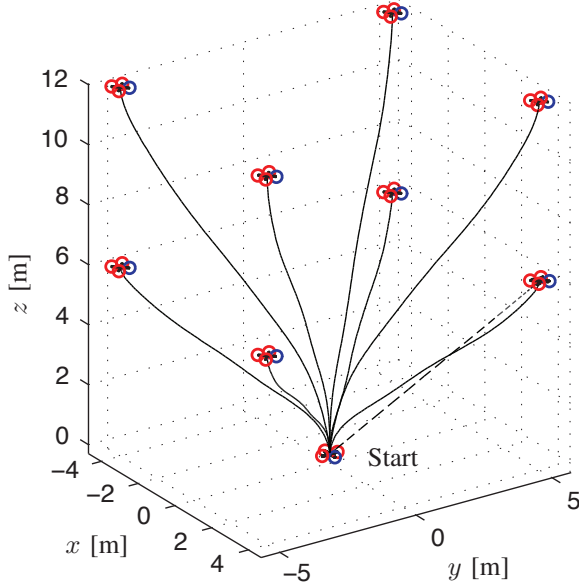


Fig. 3. **Scenario 1:** Bundle of minimum-energy trajectories of the Phantom 2 (solid lines). The dashed trajectory was generated with the controller in [25, Sect. IIIA]. To provide a reference for the reader, the propeller of motor 1 is marked in blue.

$$\begin{aligned} \mathbf{x}_{t_0} &= [\mathbf{0}_{1 \times 12}, \omega_h, \omega_h, \omega_h, \omega_h]^T, \\ \mathbf{x}_{t_f} &= [x_f, 0, y_f, 0, z_f, \mathbf{0}_{1 \times 5}, \pi/4, 0, \omega_h, \omega_h, \omega_h, \omega_h]^T, \end{aligned} \quad (13)$$

where $x_f \in \{-4, 4\}$ m, $y_f \in \{-5, 5\}$ m, and $z_f \in \{6, 12\}$ m. By considering the maximum all-up weight of 1.3 kg, $\omega_h = 912.109$ rad/s $\simeq 8710$ rpm is the angular velocity of the four propellers necessary to counterbalance the acceleration due to gravity so that the quadrotor hovers on the spot. Note that at time t_0 the vehicle is not at rest at $(0, 0, 0)$: the four propellers spin at 912.109 rad/s. Moreover, with the boundary states in (13), the condition of Remark 2 is met. Fig. 3 shows the eight minimum-energy trajectories of the Phantom 2 (solid lines). Fig. 4 reports the time-evolution of the state variables $x_1(t), \dots, x_{16}(t)$ and control inputs $\alpha_1(t), \dots, \alpha_4(t)$ relative to the two paths with $[x_f, y_f, z_f]^T = [4, 5, 6]^T$ (solid line), and $[x_f, y_f, z_f]^T = [4, 5, 12]^T$ (dashed line). The energy consumption of the quadrotor along the first path is 26.2372 kJ. If we utilize the KiBaM in (11) with $\gamma = 0.85$ and $k_F = 4.5 \times 10^{-5}$ Hz (cf. [20]) for this path, we find that $y_1(t_0) = 15912$ As and that $y_1(t_f) = 14054$ As, corresponding to a 11.67% discharge of the battery.

In order to quantify the net energy saving with our approach, we also generated a trajectory for the quadrotor using the control strategy in [25, Sect. IIIA] (see the dashed line in Fig. 3). We thus designed a sliding-mode controller for the translational dynamics, $\boldsymbol{\nu} = m([\mathbf{0}, 0, g]^T - k_1 \dot{\mathbf{q}} - k_2(\mathbf{q} - \mathbf{q}_d) - k_3 \text{Sgn}(\boldsymbol{\sigma}))$, where $\|\boldsymbol{\nu}\|_2 = u_1$ is the total thrust from the motors, $\mathbf{q}_d = [x_f, y_f, z_f]^T = [4, 5, 6]^T$, k_1, k_2 and k_3 are positive control gains, and the switching function $\boldsymbol{\sigma} = [\sigma_1, \sigma_2, \sigma_3]^T = k_1(\mathbf{q} - \mathbf{q}_d) + k_2 \int (\mathbf{q} - \mathbf{q}_d) dt + \dot{\mathbf{q}}$ where the vector sign function $\text{Sgn}(\boldsymbol{\sigma}) \triangleq [\text{sgn}(\sigma_1), \text{sgn}(\sigma_2), \text{sgn}(\sigma_3)]^T$. For the attitude stabilization, instead, we used the proportional-derivative controller $\boldsymbol{\tau} = -k_{po}(\boldsymbol{\Phi} - \boldsymbol{\Phi}_d) - k_{do} \dot{\boldsymbol{\Phi}}$ where $\boldsymbol{\tau}$ is the vector of generalized torques defined in $\{\mathcal{B}\}$, k_{po}, k_{do} are positive control gains and $\boldsymbol{\Phi}_d = [\phi_d, \theta_d, \psi_d]^T$ with $\psi_d = \pi/4$ (the desired

yaw angle), and $\phi_d = \arcsin\left(-\frac{\nu_{n2} - \nu_{n1} \tan \psi_d}{\sin \psi_d \tan \psi_d + \cos \psi_d}\right)$, $\theta_d = \arcsin\left(\frac{\nu_{n1} - \sin \phi_d \sin \psi_d}{\cos \phi_d \cos \psi_d}\right)$, being $\boldsymbol{\nu}_n = [\nu_{n1}, \nu_{n2}, \nu_{n3}]^T \triangleq \boldsymbol{\nu} / \|\boldsymbol{\nu}\|_2$. By selecting $k_1 = k_2 = 3$, $k_3 = 0.1$, $k_{po} = k_{do} = 0.75$ and by leveraging the formulae for solving for the squared angular velocities of the motors from the computed total thrust and torques [16, Sect. 2.2.2], we obtained an energy consumption of 27.0168 kJ, which corresponds to a 0.7796 kJ increase with respect to the minimum-energy path.

B. Scenario 2: variable payload

In the second scenario, we computed the minimum-energy control input of the Phantom 2 with variable payload. We first solved problem (10) by setting $m = 1.3$ kg, and by selecting \mathbf{x}_{t_0} and \mathbf{x}_{t_f} as in (13) with $[x_f, y_f, z_f]^T = [4, 5, 6]^T$ and $\omega_h = 912.109$ rad/s. Problem (10) was then solved with $m = 1$ kg (the dry weight, i.e. the weight of the quadrotor including the battery, with zero payload), \mathbf{x}_{t_0} and \mathbf{x}_{t_f} as above but with $\omega_h = 800.059$ rad/s $\simeq 7640$ rpm, which is the angular velocity of the four propellers necessary to counterbalance the acceleration due to gravity when the payload is zero. In solving problem (10) twice, we used the same t_0, t_f , and number of control intervals as in Scenario 1. Fig. 5(a) shows the trajectories of the quadrotor projected onto the xz plane, and Figs. 5(b)-(f) report the time history of the corresponding state variables of the Phantom 2 with maximum payload (solid line) and zero payload (dashed line). The energy consumed by the quadrotor along the second trajectory is 20.5513 kJ, which is smaller than 26.2372 kJ (cf. Scenario 1), as expected.

C. Scenario 3: minimum-time fixed-energy path

In the third scenario, we solved problem (12) with $\eta = 1$, $\mathbf{Q} = \mathbf{0}_{4 \times 4}$, $E_{\text{tot}} = 22$ kJ, $m = 1.3$ kg and $\mathbf{x}_{t_0}, \mathbf{x}_{t_f}$ as in (13), with $t_0 = 0$ s, $[x_f, y_f, z_f]^T = [4, 5, 6]^T$ and $\omega_h = 912.109$ rad/s. The number of control intervals was set to 60 in this case. Fig. 6(a) reports the minimum-time fixed-energy trajectory of the quadrotor, and Figs. 6(b)-(f) show the time evolution of the corresponding state variables and control inputs. The optimal value of the open end time t_f is 16.7704 s, and as it is evident from Fig. 6(a), the Phantom 2 travels along a path that is far from being minimum-length. Differently from Scenarios 1 and 2, the actuators are more solicited in this case, leading to the saturation, at $\omega_{\text{max}} = 1047.197$ rad/s $\simeq 10000$ rpm, of the angular velocity of the motors (see Fig. 6(e)). In spite of this, the physical constraints of the Phantom 2 ($\theta \leq 0.6109$ rad, $\dot{\psi} \leq 3.4907$ rad/s, maximum flight speed 15 m/s), are not violated.

As a concluding remark, note that the computation time with the ACADO Toolkit under Matlab 7.9 is, on average, 86.75 s for Scenarios 1 and 2, and 68.09 s for Scenario 3 on a MacBook Pro with 4 GB RAM and 2.53 GHz Intel Core 2 Duo CPU. This is not critical in practice, since the energy-optimal trajectories can be computed offline and stored in the memory of the quadrotor as a sequence of waypoints. However, in certain situations (if the environment is not known a priori or is highly dynamic, if the boundary states are largely spaced), it might be preferable to find *approximate* solutions to problems (10) and (12), e.g. via a receding-horizon approach, using the on-board computational power of the quadrotor. This is the subject of ongoing research.

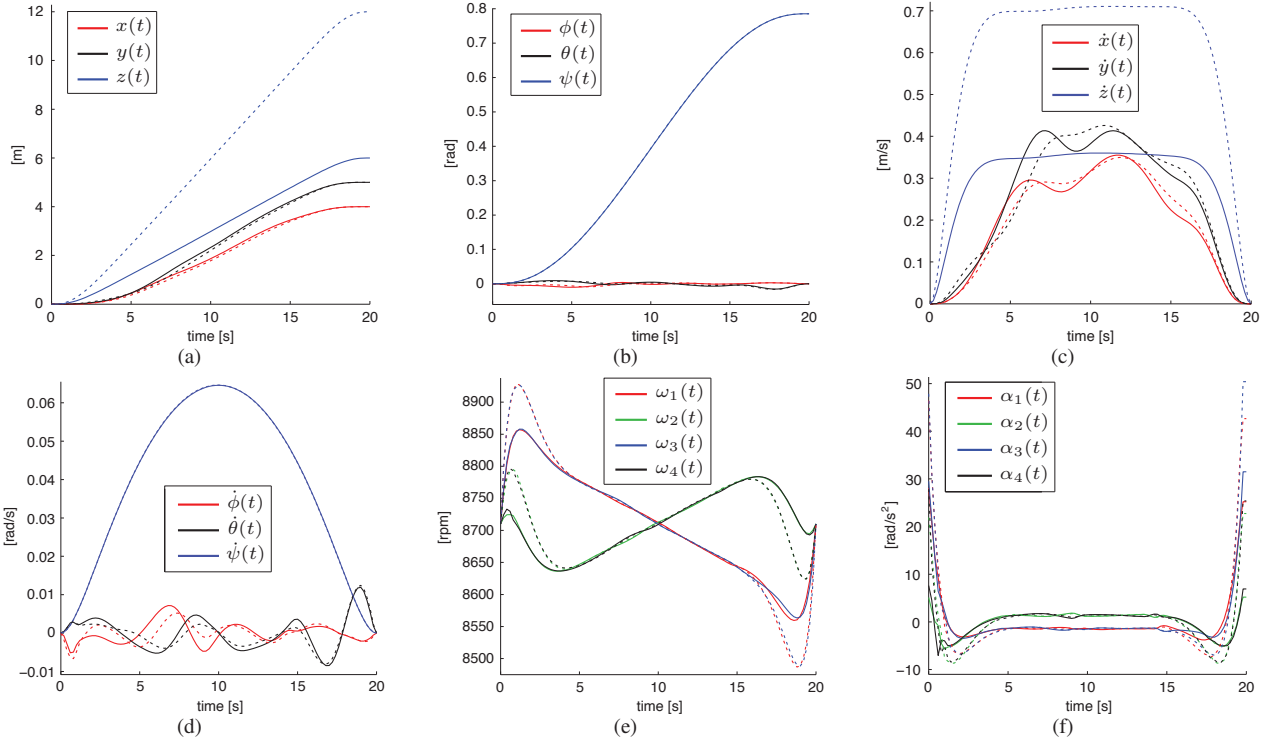


Fig. 4. **Scenario 1:** Time evolution of the state variables and control inputs of the Phantom 2 for $[x_f, y_f, z_f]^T = [4, 5, 6]^T$ (solid line), and $[x_f, y_f, z_f]^T = [4, 5, 12]^T$ (dashed line).

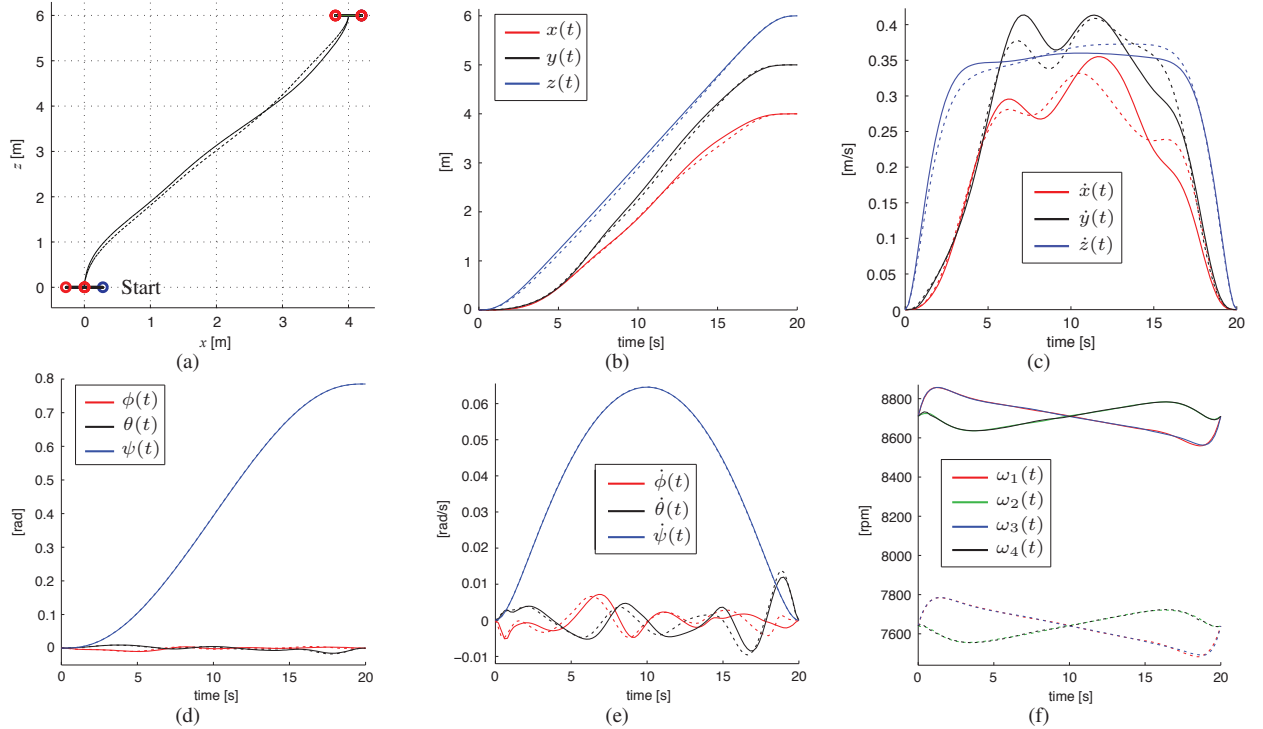


Fig. 5. **Scenario 2:** (a) Trajectories of the Phantom 2 projected onto the xz plane, and (b)-(f) time evolution of the corresponding state variables for $m = 1.3$ kg (solid line), and $m = 1$ kg (dashed line).

V. CONCLUSIONS AND FUTURE WORK

Motivated by the limited flight endurance of the existing battery-powered quadrotor UAVs, in this paper we have

introduced two new optimal control problems with respect to the angular accelerations of the four electrical motors. Their solution yielded minimum-energy and fixed-energy

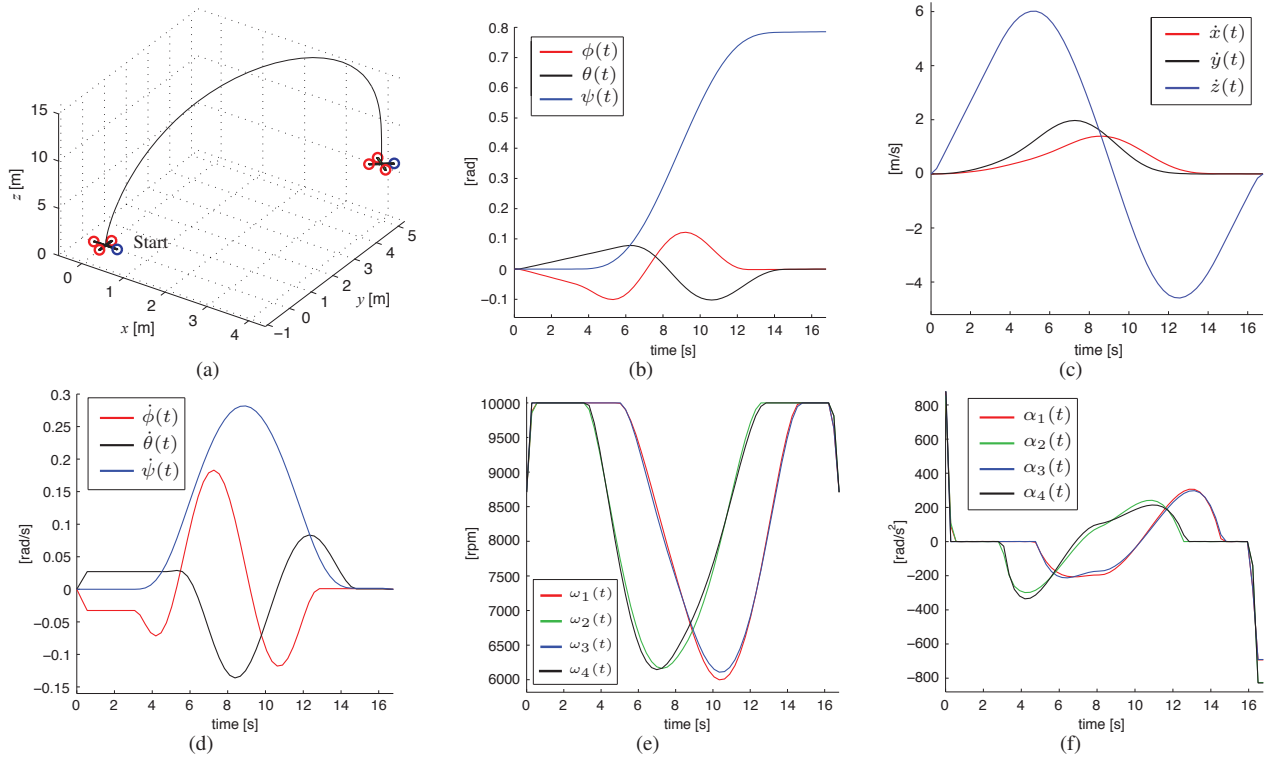


Fig. 6. **Scenario 3:** (a) Minimum-time fixed-energy trajectory of the Phantom 2 ($E_{\text{tot}} = 22$ kJ), and (b)-(f) time evolution of the corresponding state variables and control inputs.

paths for the aerial vehicle. The proposed theory has been illustrated via numerical experiments conducted with the DJI Phantom 2 quadrotor.

In future works, we will incorporate in our problems, sources of energy consumption other than the DC motors (e.g. the ESC and the microcontroller), and we will analyze the robustness of the proposed approach against model uncertainty and external disturbances. We are also going to devise a simple experimental procedure to identify the six constants in the cost function (8), and we are interested in extending our results to determine energy-efficient paths for multiple quadrotors flying in tight formation.

REFERENCES

- [1] S. Driessens and P. Pounds. The Triangular Quadrotor: A More Efficient Quadrotor Configuration. *IEEE Trans. Robot.*, 31(6):1517–1526, 2015.
- [2] M. Ryll, H.H. Bulthoff, and P. Robuffo Giordano. A Novel Overactuated Quadrotor Unmanned Aerial Vehicle: Modeling, Control, and Experimental Validation. *IEEE Trans. Contr. Syst. Tech.*, 23(2):540–556, 2015.
- [3] D. Gurdan, J. Stumpf, M. Achtelik, K.-M. Doth, G. Hirzinger, and D. Rus. Energy-efficient Autonomous Four-rotor Flying Robot Controlled at 1 kHz. In *Proc. IEEE Int. Conf. Robot. Automat.*, pages 361–366, 2007.
- [4] J.F. Roberts, J.-C. Zufferey, and D. Floreano. Energy Management for Indoor Hovering Robots. In *Proc. IEEE/RSJ Int. Conf. Intel. Robots Syst.*, pages 1242–1247, 2008.
- [5] A. Abdilla, A. Richards, and S. Burrow. Power and Endurance Modelling of Battery-Powered Rotorcraft. In *Proc. IEEE/RSJ Int. Conf. Intel. Robots Syst.*, pages 675–680, 2015.
- [6] T. Chang and H. Yu. Improving Electric Powered UAVs’ Endurance by Incorporating Battery Dumping Concept. *Procedia Engineering*, 99:168–179, 2015.
- [7] T. Lee. Geometric Controls for a Tethered Quadrotor UAV. In *Proc. 54th IEEE Conf. Dec. Contr.*, pages 2749–2754, 2015.
- [8] J. Leonard, A. Savvaris, and A. Tsourdos. Energy Management in Swarm of Unmanned Aerial Vehicles. *J. Intell. Robot. Syst.*, 74(1-2):233–250, 2014.
- [9] N. Kemal Ure, G. Chowdhary, T. Toksoz, J.P. How, M. Vavrina, and J. Vian. An Automated Battery Management System to Enable Persistent Missions with Multiple Aerial Vehicles. *IEEE-ASME Trans. Mech.*, 20(1):275–286, 2015.
- [10] K. Vicencio, T. Korrás, K.A. Bordignon, and I. Gentilini. Energy-Optimal Path Planning for Six-Rotors on Multi-Target Missions. In *Proc. IEEE/RSJ Int. Conf. Intel. Robots Syst.*, pages 2481–2487, 2015.
- [11] P. Tokekar, N. Karnad, and V. Isler. Energy-optimal trajectory planning for car-like robots. *Auton. Robot.*, 37(3):279–300, 2014.
- [12] D. Ariens, B. Houska, H. Ferreau, and F. Logist. ACADO: Toolkit for Automatic Control and Dynamic Optimization, 2010.
- [13] Electro-Craft Corp. USA. *DC Motors, Speed controls, Servo Systems: An Engineering Handbook*. Pergamon Press, 3rd edition, 1977.
- [14] J.F. Gieras. *Permanent Magnet Motor Technology: Design and Applications*. CRC press, 3rd edition, 2010.
- [15] S. Bouabdallah, P. Murrieri, and R. Siegwart. Towards Autonomous Indoor Micro VTOL. *Auton. Robot.*, 18(2):171–183, 2005.
- [16] L.R. Carrillo, A.E. López, R. Lozano, and C. Pégard. *Quad Rotorcraft Control: Vision-Based Hovering and Navigation*. Springer, 2013.
- [17] R. Mahony, V. Kumar, and P. Corke. Multirotor Aerial Vehicles: Modeling, Estimation, and Control of Quadrotor. *IEEE Rob. Autom. Mag.*, 19(3):20–32, 2012.
- [18] J.G. Leishman. *Principles of Helicopter Aerodynamics*. Cambridge University Press, 2nd edition, 2006.
- [19] D.E. Kirk. *Optimal Control Theory: An Introduction*. Dover Pub., 2004.
- [20] M.R. Jongerden and B.R. Haverkort. Which battery model to use? *IET Softw.*, 3(6):445–457, 2009.
- [21] R.F. Stengel. *Optimal Control and Estimation*. Dover Pub., 1994.
- [22] DJI Phantom 2. [web]: www.dji.com/product/phantom-2.
- [23] P. Pounds, R. Mahony, and P. Corke. Modelling and Control of a Large Quadrotor Robot. *Control Eng. Pract.*, 18(7):691–699, 2010.
- [24] M. Cutler, N. Kemal Ure, B. Michini, and J.P. How. Comparison of Fixed and Variable Pitch Actuators for Agile Quadrotors. In *Proc. AIAA Conf. Guidance, Navig. Contr.*, 2011. Paper 6406.
- [25] D.A. Mercado, R. Castro, and R. Lozano. Quadrotors Flight Formation Control Using a Leader-Follower Approach. In *Proc. European Contr. Conf.*, pages 3858–3863, 2013.